RESEARCH ARTICLE | OCTOBER 24 2024

Microsphere-enhanced fluorescence collection for nitrogen vacancy centers in diamond

Shu-Hao Wu ; Ignas Lekavicius ; Hailin Wang

Appl. Phys. Lett. 125, 171109 (2024)
https://doi.org/10.1063/5.0230091

Applied Physics Letters ARTICLE pubs.aip.org/aip/apl

Microsphere-enhanced fluorescence collection for nitrogen vacancy centers in diamond

Cite as: Appl. Phys. Lett. **125**, 171109 (2024); doi: 10.1063/5.0230091
Submitted: 21 August 2024 · Accepted: 14 October 2024 ·
Published Online: 24 October 2024

Shu-Hao Wu,[a] Ignas Lekavicius, and Hailin Wang

AFFILIATIONS

Department of Physics, University of Oregon, Eugene, Oregon 97403, USA

[a]Author to whom correspondence should be addressed: swu8@uoregon.edu

ABSTRACT

We report experimental studies of microsphere-enhanced fluorescence collection of nitrogen vacancy (NV) centers using silica microspheres with diameters ranging between 15 and 50 μm and employing 20× and 40× objectives with numerical aperture of 0.42 and 0.64, respectively. Photoluminescence-excitation saturation counts as high as 95 kHz have been observed. These studies show that due to the effective collimation of fluorescence by the microsphere, objectives with relatively low numerical aperture (NA) can be used without sacrificing collection enhancement, in agreement with a theoretical model based on Mie scattering. The large enhancement of fluorescence collection with relatively low NA objectives, which feature extralong working distance and are relatively inexpensive, can potentially enable wider use of NV-based quantum sensing in real world applications.

Color centers in diamond, especially, nitrogen vacancy (NV) centers, are one of the most widely used systems for quantum sensing.[1,2] NV-based quantum sensing has been employed for measurements of magnetic field, electric field, temperature, and strain with nanometer spatial resolution.[3–6] The poor collection efficiency of fluorescence from these emitters, however, limits their real-world applications. This inefficiency primarily arises from the substantial mismatch in the refractive index between diamond and air such that a large fraction of the emission from color centers undergoes total internal reflection at the interface. A variety of optical techniques, such as diamond solid immersion lens (SIL),[7] diamond nanopillars,[8] and metalenses,[9] have been exploited to overcome this limitation. These techniques require costly nanofabrication and/or precise positioning of the color centers. For diamond SIL, which is the standard approach for enhancing fluorescence collection, the color center needs to be at or near the center of a hemisphere with a radius of several micrometers, making it unsuitable for applications where the color center needs to be within tens or at least hundreds of nm from the diamond surface. Furthermore, the non-directional nature of fluorescence necessitates the use of a high numerical aperture (NA) objective, which is expensive and has a working distance (WD) of a few mm or shorter, to achieve the necessary collection efficiency, limiting practical applications.

Dielectric microspheres have been used in super-resolution imaging, conveying high-frequency information to the far field when placed near the object.[10] These studies also suggest the potential for microsphere-enhanced fluorescence collection. Enhanced collections using microspheres have been demonstrated for quantum dots[11,12] as well as NV centers in diamonds,[13] demonstrating significant improvements in collection efficiency as well as a reduction in saturation power for optical excitation of NV centers. Nevertheless, a few important issues remain to be addressed. There have been no investigations on the microsphere size dependence. More importantly, it is not clear whether near optimal performance of microsphere-enhanced fluorescence collection can be achieved with low-NA objectives, which are relatively inexpensive and can feature WD exceeding several centimeters. A quantitative theoretical description of the enhancement has also been lacking.

Here, we report experimental studies of microsphere-enhanced fluorescence collection of NV centers using silica microspheres with diameters ranging between 15 and 50 μm and employing 40× and 20× objectives. The experimental results are compared with a theoretical model based on Mie scattering. Photoluminescence excitation (PLE) saturation counts as high as 95 kHz have been observed with the 20× objective, which surpasses the maximum saturation counts of 60–80 kHz typically achieved with a 0.95 NA objectives and with no enhanced collection.[7,14,15] We show that due to the effective collimation of fluorescence by a microsphere, relatively low NA objectives can be used without sacrificing collection enhancement. Our theoretical analysis confirms the experimental observation and indicates that for the size of the microspheres used, the enhancement is primarily due to

geometric optical processes, with minor contributions from evanescent coupling between whispering gallery modes (WGMs) and the NV centers.

We fabricated silica microspheres by melting the tip of an optical fiber using a CO_2 laser. By controlling the laser power and the duration of melting, we can achieve a desired diameter ranging from 10 to 100 μm. The remaining fiber stem attached to the microsphere helps transport it to any position on the diamond sample with a vacuum pickup tweezer. A tight contact between the microsphere and the sample surface can be confirmed with the observation of a Newton ring pattern, as shown in the lower right corner of Fig. 1. Van der Waals forces secure the microsphere in place throughout the experiment. More elaborate methods involve gluing the fiber stem to a fixed position and moving the sample with nanopositioners or using an optical tweezer to position a microsphere without stems,[13] showcasing the flexibility for *in situ* positioning of a microsphere. The type IIa [100] diamond sample used is from Element 6, Inc. The NV centers were created about 100 nm below the surface through ion implantation, followed by stepwise high temperature thermal annealing and wet chemical oxidation.

A standard confocal optical setup is employed for photoluminescence (PL) and photoluminescence excitation (PLE) measurements of the NV center, as illustrated in Fig. 1. The diamond sample is cooled to cryogenic temperatures (near 5 K) and excited with a non-resonant 532 nm laser for PL or a resonant 637 nm laser for PLE. For PLE studies, we scan the 637 nm laser across E_x transition of the NV center by tuning a voltage based on feedback from a wavemeter. The fluorescence from the NV centers is sent through a 90:10 beam splitter and a 650 nm long-pass filter and then coupled into a multi-mode (MM) optical fiber connected to an avalanche photodiode (APD). While dependences on microsphere sizes, objective NAs, and MM fiber core diameters are investigated in this work, a 50 μm MM fiber, 25 μm microsphere, and 40× objective are used in the experimental results presented here unless otherwise specified.

A confocal PL imaging of NV centers obtained with the use of a silica microsphere is shown in the lower left of Fig. 1, where individual NV centers are identified within the contact area. We also conducted a $g^{(2)}$ time correlation experiment for one of the NV centers using a 50:50 fiber splitter and two APDs, the result of which is shown in the upper left of Fig. 1. The dashed gray line indicates the 0.5 criterion for single-photon emitters. The dashed black line denotes the estimated background correlation arising from background counts. Note that PL counts of NV centers depend on the relative position of the NV centers to the center of the contact area. For studies of microsphere size dependence, we chose two individual NV centers under each sphere, which exhibit relatively high count rates.

To quantify the enhanced collection provided by a microsphere, the most common method is to use PL saturation counts.[11,13] For our studies, this approach is complicated by the background counts from nearby NV centers, especially when relatively high optical excitation powers are used. In comparison, PLE saturation counts of the NV center are unaffected by background counts, as we can always perform curve fitting in PLE spectra and extract the background-free peak PLE counts, as shown in Fig. 2(a). Figure 2(b) shows the saturation of the peak PLE counts with increasing optical excitation powers. The saturation is expressed in the following equation:

$$I = I_{\text{sat}}\left(\frac{P/P_{\text{sat}}}{1 + P/P_{\text{sat}}}\right), \tag{1}$$

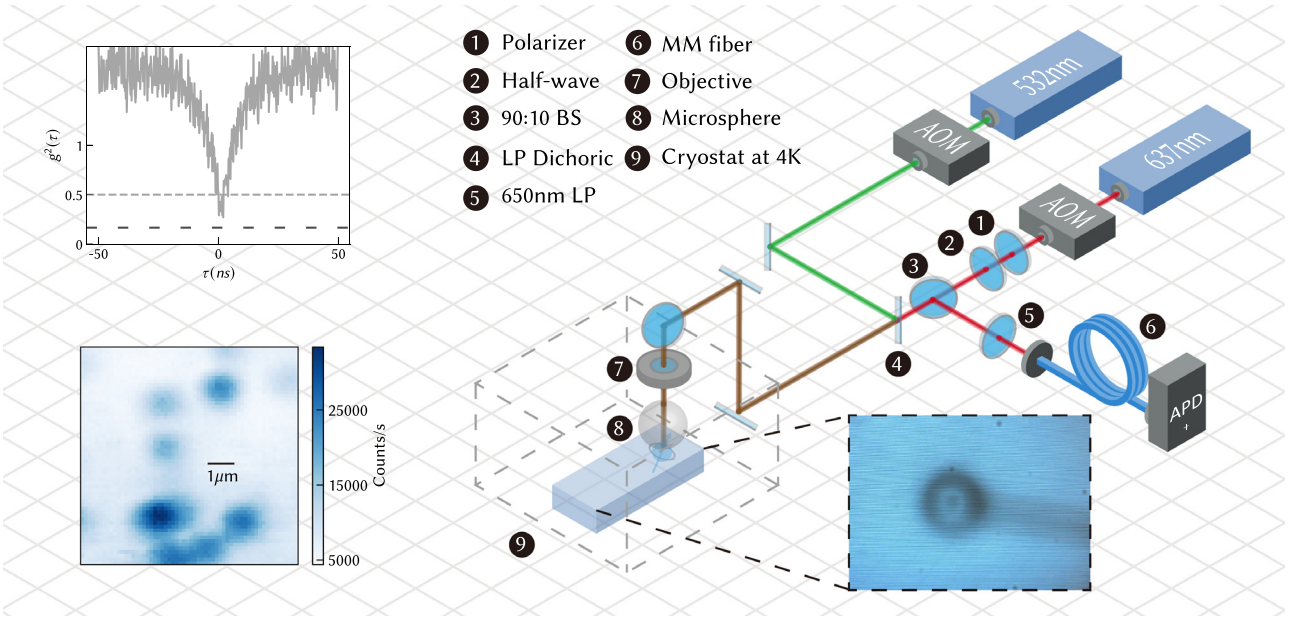

FIG. 1. Experimental setup for microsphere-enhanced fluorescence collection. Right: A confocal optical setup. A microsphere is positioned above the diamond membrane. The observation of a Newton's ring pattern confirms a tight contact. A 637 nm laser is used for the resonant excitation of the E_x transition of the NV centers, while a 532 nm laser is pulsed occasionally to initialize the NV centers and to stabilize the charge state. The fluorescence's phonon sidebands are collected through a 650 nm long-pass filter. Lower left: Confocal PL imaging of NV centers under the microsphere, obtained under non-resonant optical excitation. Upper left: Time-correlation measurement, carried out with a 50:50 fiber splitter and two APDs.

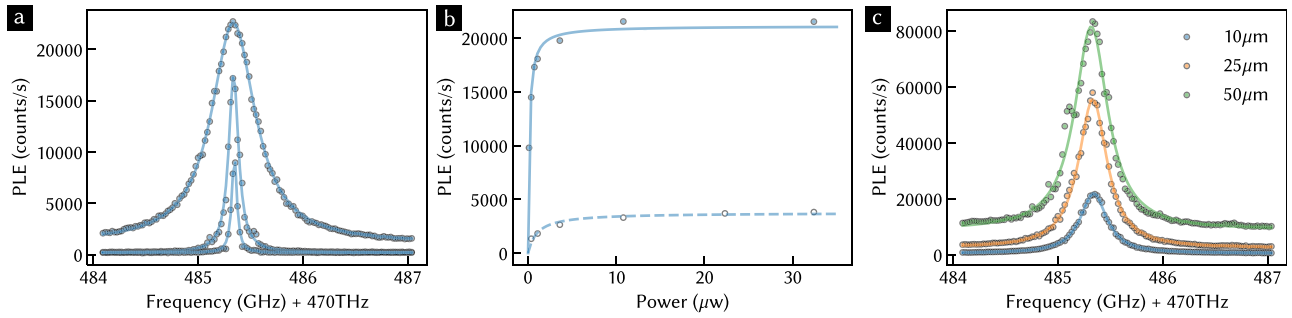

FIG. 2. Photoluminescence excitation spectra and saturation photon counts. (a) PLE spectra with increasing optical power (0.11, 1.1, and 32.4 μW) showing power broadening, saturation, and increasing background contributions. The data were obtained with a 25 μm diameter microsphere and 10 μm diameter MM fiber. Solid lines are the least squares fit to a Lorentzian. (b) Peak PLE counts extracted from the corresponding PLE spectra vs the optical excitation power. Solid (open) circles are data obtained with (without) a microsphere and with a 10 μm diameter MM fiber. Solid and dashed lines are numerical fits to the equation in the text. (c) PLE spectra obtained with an optical power of 10.8 μW and with a MM fiber featuring a diameter of 10, 25, and 50 μm, as indicated in the figure, showing reduced background contribution as well as reduced collection efficiency with decreasing fiber diameters.

where I_{sat} and P_{sat} represent the saturation counts for PLE and the saturation optical power, respectively. Theoretically, the saturation counts are determined by spontaneous decay rate of the NV center, Γ, which should be uniform among different samples, and collection efficiency, η, by $I_{sat} = \eta\Gamma/2$, thus providing a robust approach to extract and compare collection efficiency from the saturation curve. For comparison, Fig. 2(b) presents the saturation curves obtained with and without the use of a microsphere, indicating that the use of a microsphere enhances the collection efficiency by a factor of 5.7 and reduces saturation power by a factor of 7. The reduction in the saturation power, or in other words, the super-focusing or photonic nanojet effect, is related to the microsphere's ability to focus a laser beam beyond the diffraction-limited spot size. This effect, discussed in Ref. 16, plays a significant role in super-resolution imaging using microspheres.[10] Note that different NV centers were used for the two curves in Fig. 2(b) because of the difficulties of tracking the same NV center during positioning of the microsphere. It should also be added that the background counts in PLE can be reduced with the use of MM fibers of smaller diameters, though with a corresponding decrease in the overall collection efficiency (which is in large part due to the nonoptimal optical alignment for coupling fluorescence into the MM fiber), as shown in Fig. 2(c).

Figure 3 shows the saturation PLE counts as well as PLE spectra obtained with microspheres featuring three different sizes and objectives featuring two different NAs. As shown in Fig. 3(a), saturation counts as high as 95 kHz are observed with a 25 μm sphere and a 20× objective (NA = 0.42). For comparison, typical saturation PL counts are around 60–80 kHz with a 0.95 NA objective and without enhanced collection,[7,14,15] and the corresponding PLE saturation counts are expected to be even lower. Our maximum saturation counts represent an 11.4-fold enhancement over the saturation counts obtained without a microsphere under otherwise the same conditions, surpassing the theoretical enhancement of 6.11 provided by diamond SIL under otherwise the same conditions.[7] Because of the different lateral offsets of NVs to the center of the respective contact area as well as the variations in the optical alignment when different microspheres are used, Fig. 3(a) does not provide conclusive results on the dependence of the enhancement in florescence collection on the microsphere diameter. Nevertheless, there does not seem to be evidence for strong size dependence.

Given that the enhancement could be affected by non-optimal alignment without a microsphere, a comparison of absolute saturation counts is beneficial. From the state-of-the-art saturated PL counts of near 1 MHz for NV centers in [111] orientation diamond and the theoretical simulation of diamond SIL,[17] we estimate a 133 kHz PL saturation count under a 20× objective with the SIL. Considering the differences between PL and PLE, the orientation of the diamond, and potential alignment issues in our experiment, the 95 kHz PLE saturation count achieved with a silica microsphere and a 20× objective is noteworthy.

In addition, Fig. 3(a) shows that despite variations due to misalignment during changes of objectives, both the 20× and 40× objectives yield similar saturation counts. For a more detailed comparison, Figs. 3(b) and 3(c) show saturated PLE spectra obtained with an optical power of 10.8 μW and with a microsphere of 25 and 15 μm in diameter, respectively, which indicate that the 20× objective enables similar collection efficiency as the 40x. In addition to the much-reduced cost, the use of a 20× objective with a WD of several centimeters is especially important for applications that require a long WD. Overall, these studies suggest that after collimation by the microsphere, optical emissions from a NV center become highly directional, which we will discuss in more detail in the following theoretical analysis based on Mie scattering.

We have developed a theoretical model to describe microsphere-enhanced fluorescence collection by using Mie scattering. Earlier theoretical analysis has largely relied on finite element (FEM) numerical simulations. The Mie scattering approach provides a rigorous solution to Maxwell's equations, describing the scattering of a plane wave by a sphere. In this context, we follow the notations from,[18,19] which include a modified Mie scattering problem with reflection from a nearby planar surface. To simplify the Mie solution without losing generality, we model the emission from the NV center as a spherical wave with radial polarization. Fully numerical results on the dipole radiation wave collection and its dependence on dipole orientations can be found in earlier studies.[13] By applying the plane wave decomposition (Weyl expansion) to the spherical wave and considering the Fresnel reflection at the interface, we derive the plane wave expression of the emission from the NV center after diamond–air surface as

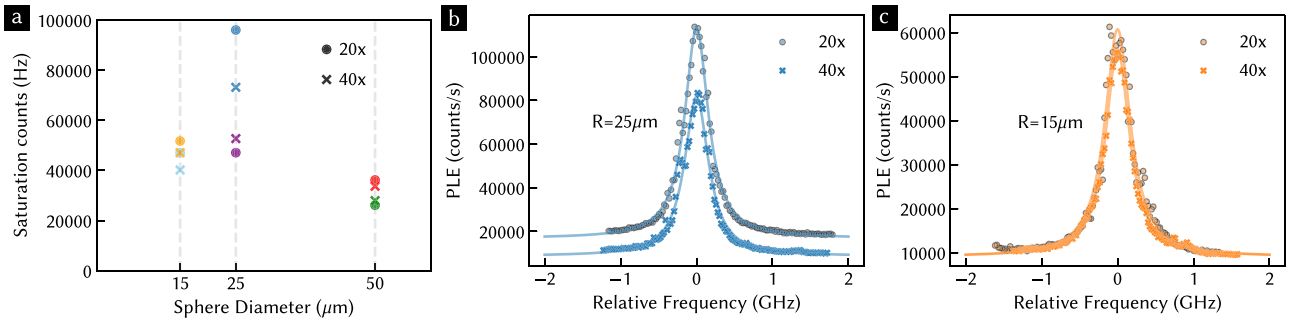

FIG. 3. Dependence of saturation photon counts on microsphere size and objective NA. (a) Saturation PLE counts obtained with microspheres with three different diameters and objectives with two different NAs, with each color representing a different NV center. (b) and (c) PLE spectra obtained with an optical power of 10.8 μW and with a microsphere with 25 and 15 μm in diameter, respectively. Saturation counts extracted from the PLE spectra are also shown in (a).

$$\mathbf{E}_i(\mathbf{r}) = \int \mathbf{e}_\theta e^{i\mathbf{kr}} d\theta d\varphi = \sum_{n=1}^{\infty} \frac{(-i)^{n+1}(2n+1)2\pi}{n(n+1)} a_n^i N_{0n}^1(k\mathbf{r}), \quad (2)$$

where

$$a_n^i = \int \sin(\theta) P_n^1(\cos\theta_t) e^{ikR\cos\theta_t} \frac{2n_d\cos\theta}{\cos\theta + n_d\cos\theta_t} d\theta, \quad (3)$$
$$\theta_t = \sin^{-1}(n_d \sin\theta).$$

The corresponding scattered field is

$$\mathbf{E}_s(\mathbf{r}) = \sum_{n=1}^{\infty} \frac{(-i)^{n+1}(2n+1)2\pi}{n(n+1)} a_n^s N_{0n}^3(k\mathbf{r}), \quad (4)$$

where

$$a_n^s = -a_n^i \frac{n_s^2(\rho j_n(\rho))' j_n(\rho_1) - (\rho_1 j_n(\rho_1))' j_n(\rho)}{n_s^2(\rho h_n(\rho))' j_n(\rho_1) - (\rho_1 j_n(\rho_1))' h_n(\rho)}, \quad (5)$$
$$\rho = kR, \quad \rho_1 = n_s kR,$$

$N_{0n}^{(i)}(k\mathbf{r})$ denotes the vector spherical harmonics with i-kind radial function, and k, n_d, n_s, R denote the wave vector, refractive index of diamond, refractive index of the sphere, and sphere radius, respectively. By estimating the total field $\mathbf{E}_i + \mathbf{E}_s$ at a far distance, we can determine the angular distribution of the optical emission power. Although the above-mentioned analysis is valid for complex angles and the associated Legendre function has its complex extension, the scattering of evanescent waves resulting from the total internal reflection at the surface does not converge to a physically meaningful result. This indicates that we cannot overlook multiple reflections from the surface, especially for evanescent waves. Considering the modified Mie scattering solution mentioned above, we can incorporate the effect of the surface by evaluating it using an additional inverse matrix.[18] The scattering of evanescent waves exhibits peaks at whispering gallery mode (WGM) resonances or morphology dependent resonances (MDR)[20] as shown in Fig. 4(a), where a considerable amount of evanescent wave energy is converted into propagating waves and brought to the far field. This, along with averaging the collection over the emission spectrum of the NV center, leads to an additional enhancement of

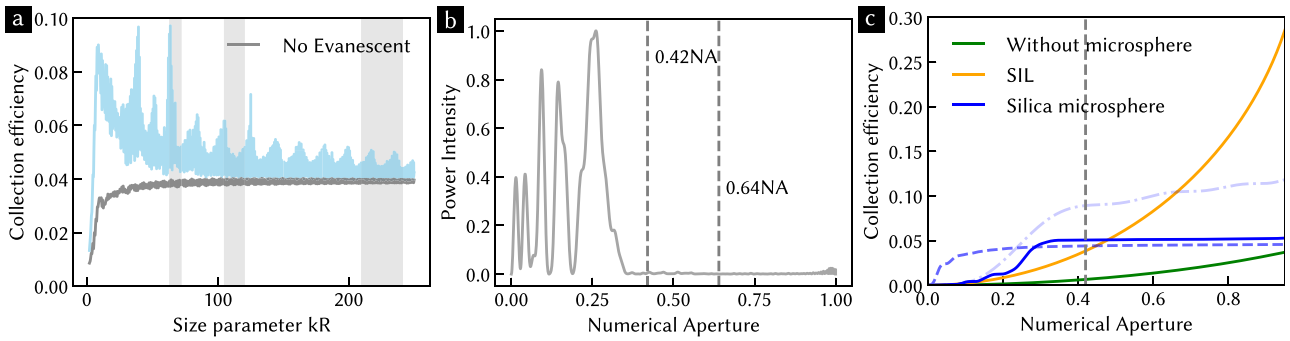

FIG. 4. Theoretically calculated collection efficiency and angular distribution. (a) Theoretical collection efficiency (blue curve) obtained with the use of a silica microsphere and a 0.42 NA objective. The size parameter kR is the product of the wavevector and microsphere radius. The gray curve denotes the same simulation but removes contributions from evanescent waves. For a NV center with an emission spectrum from 650 to 750 nm, the collection efficiency can be obtained by averaging a given shaded area in the figure, which corresponds to microspheres with diameters of 15, 25, and 50 μm, respectively. (b) Simulated angular distribution of the emission power after collimation by a microsphere. Most of the emission falls within the collection range of the 0.42 NA objective, consistent with the experimental observations. (c) Comparison of theoretical collection efficiencies for various collection approaches. The solid blue, green, and orange lines denote the collection efficiencies obtained with a silica microsphere of 25 μm in diameter, without a microsphere, and with a diamond SIL, respectively. The dot-dashed line denotes the collection efficiency for a silica microsphere with a diameter of 1.8 μm. The dashed line denotes the collection efficiency for a microsphere with a diameter of 25 μm and a refractive index of 1.8.

20%–30% over that allowed by geometrical optical processes. Our theoretical model agrees with FEM simulations and is also capable of predicting the nearly 40% enhancement observed in an earlier experiment.[13]

While the contribution from evanescent waves may be crucial for describing super-resolution imaging using a microsphere, the calculation shown in Fig. 4(a) indicates that the enhancement of fluorescence collection is primarily due to optical lensing or optical collimation, especially for the microsphere sizes used in our experiments. Specifically, the gray and blue curves in Fig. 4(a) denote the collection efficiency due to the geometric optical process and the overall collection efficiency (including contributions from both geometric optical and evanescent processes), respectively. The difference between these two curves thus represents the evanescent wave contribution. For the three microsphere sizes used in our experiment, contributions from the geometrical optical process still dominate, as shown in Fig. 4(a). The theoretical results in Fig. 4(a) are also consistent with the weak microsphere size dependence shown in Fig. 3(a). In addition, since the enhanced fluorescence collection is primarily due to geometric optical effects, we can use geometric optical formulas to estimate the collection efficiency under non-ideal conditions. For example, when the emitter is a distance d below the sample surface, geometric optics predicts a reduction by a factor of $(1 - 2.11(d/R)^2)$, up to the second order of (d/R), in the collection efficiency. This results in a nearly negligible drop in the geometric contribution for d up to 1 μm. The estimated overall reduction in the collection efficiency for d near 1 μm is 30% under our experimental conditions, making this technique applicable beyond quantum sensing applications where a shallow NV center is typically used.

In Fig. 4(b), we plot the angular dependence of the optical emission after its propagation through the microsphere. The numerical results reveal a highly directional emission pattern, with most of the emission falling within the 0.42 NA of the 20× objective, in good agreement with the experimental observation of Fig. 3. This behavior can also be understood from a geometrical optics perspective, for which fluorescence from a NV center is effectively collimated by a silica microsphere, resulting in a relatively narrow cone angle. Mie scattering simulations predict that the microsphere can redirect 95% of the emission within the critical angle into a narrow cone angle compatible with the 20× objective, with an additional contribution coming from the evanescent wave conversion. Consequently, with the use of a silica microsphere, the 20× objective can effectively outperform a 0.95 NA objective by about 50%, significantly enhancing collection efficiency, as discussed earner and confirmed by the calculation in Fig. 4(c).

Figure 4(c) compares theoretically calculated collection efficiencies for various collection approaches, providing additional physical insights. For a microsphere with a diameter of 25 μm and a refractive index of 1.8 (dashed line in the figure), optical emissions can be collimated into a narrow cone such as that an objective with a NA as small as 0.1 and a WD up to 10 cm can be used without sacrificing collection efficiency. This calculation also indicates that there is no clear advantage in using high index microspheres as long as an objective with NA > 0.3 is used. For silica microspheres with a diameter of 1.8 μm (dot-dashed line in the figure), contributions from evanescent waves lead to an overall collection efficiency, which can be nearly twice that of microspheres with a diameter of 25 μm. Furthermore, for NA < 0.45, the performance of the microsphere approach can surpass that of the diamond SIL approach.

By carrying out a systematic experimental study and developing a theoretical model based on Mie scattering, we have gained significant insights into microsphere-enhanced florescence collection. Due to the effective collimation of fluorescence by a dielectric microsphere, large enhancement in fluorescence collection can be achieved with objectives that feature relatively low NA, extra-long working distance, as well as relatively small cost. With the use of a silica microsphere, a 20× objective with NA = 0.42 can outperform a 0.95 NA objective (with no microsphere) by a considerable margin. Microsphere-enhanced florescence collection, which is not only easy to implement but also substantially lowers the total cost of the experimental setup, overcomes many of the limitations of other widely used enhancement approaches, potentially enabling wider applications of color-center based quantum sensing in real world.

This work is supported by NSF under Grant No. 2003074 and by ARO MURI under Grant No. W911NF-18-1-0218.

AUTHOR DECLARATIONS

Conflict of Interest

The authors have no conflicts to disclose.

Author Contributions

Shu-Hao Wu: Writing – original draft (equal). **Ignas Lekavicius:** Writing – review & editing (equal). **Hailin Wang:** Writing – review & editing (equal).

DATA AVAILABILITY

The data that support the findings of this study are available from the corresponding author upon reasonable request.

REFERENCES

[1]C. L. Degen, F. Reinhard, and P. Cappellaro, "Quantum sensing," Rev. Mod. Phys. **89**, 035002 (2017).
[2]V. Giovannetti, S. Lloyd, and L. Maccone, "Advances in quantum metrology," Nat. Photonics **5**, 222 (2011).
[3]J. M. Taylor, P. Cappellaro, L. Childress, L. Jiang, D. Budker, P. Hemmer, A. Yacoby, R. Walsworth, and M. Lukin, "High-sensitivity diamond magnetometer with nanoscale resolution," Nat. Phys. **4**, 810 (2008).
[4]F. Dolde, H. Fedder, M. W. Doherty, T. Nöbauer, F. Rempp, G. Balasubramanian, T. Wolf, F. Reinhard, L. C. Hollenberg, F. Jelezko *et al.*, "Electric-field sensing using single diamond spins," Nat. Phys. **7**, 459 (2011).
[5]G. Kucsko, P. C. Maurer, N. Y. Yao, M. Kubo, H. J. Noh, P. K. Lo, H. Park, and M. D. Lukin, "Nanometre-scale thermometry in a living cell," Nature **500**, 54 (2013).
[6]M. W. Doherty, V. V. Struzhkin, D. A. Simpson, L. P. McGuinness, Y. Meng, A. Stacey, T. J. Karle, R. J. Hemley, N. B. Manson, L. C. Hollenberg *et al.*, "Electronic properties and metrology applications of the diamond nv-center under pressure," Phys. Rev. Lett. **112**, 047601 (2014).
[7]P. Siyushev, F. Kaiser, V. Jacques, I. Gerhardt, S. Bischof, H. Fedder, J. Dodson, M. Markham, D. Twitchen, F. Jelezko *et al.*, "Monolithic diamond optics for single photon detection," Appl. Phys. Lett. **97**, 241902 (2010).
[8]E. Neu, P. Appel, M. Ganzhorn, J. Miguel-Sánchez, M. Lesik, V. Mille, V. Jacques, A. Tallaire, J. Achard, and P. Maletinsky, "Photonic nano-structures on (111)-oriented diamond," Appl. Phys. Lett. **104**, 153108 (2014).
[9]T.-Y. Huang, R. R. Grote, S. A. Mann, D. A. Hopper, A. L. Exarhos, G. G. Lopez, A. R. Klein, E. C. Garnett, and L. C. Bassett, "A monolithic immersion metalens for imaging solid-state quantum emitters," Nat. Commun. **10**, 2392 (2019).

[10]L. A. Krivitsky, J. J. Wang, Z. Wang, and B. Luk'yanchuk, "Locomotion of microspheres for super-resolution imaging," Sci. Rep. **3**, 3501 (2013).
[11]F. Biccari, T. Hamilton, A. Ristori, S. Sanguinetti, S. Bietti, M. Gurioli, and H. Mohseni, "Quantum dots luminescence collection enhancement and nanoscopy by dielectric microspheres," Part. Part. Syst. Charact. **37**, 1900431 (2020).
[12]L. Yang, L. Li, Q. Wang, C. Xing, L. Ma, Y. Zeng, Y. Zhao, and Y. Yan, "Over 1000-fold enhancement of the unidirectional photoluminescence from a microsphere-cavity-array-capped QD/PDMS composite film for flexible lighting and displays," Adv. Opt. Mater. **7**, 1901228 (2019).
[13]J. S. Moon, H. Lee, J. H. Lee, W. B. Jeon, D. Lee, J. Lee, S. Paik, S.-W. Han, R. Reuter, A. Denisenko *et al.*, "High-resolution, high-contrast optical interface for defect qubits," ACS Photonics **8**, 2642 (2021).
[14]I. Lovchinsky, A. Sushkov, E. Urbach, N. P. de Leon, S. Choi, K. De Greve, R. Evans, R. Gertner, E. Bersin, C. Müller *et al.*, "Nuclear magnetic resonance detection and spectroscopy of single proteins using quantum logic," Science **351**, 836 (2016).
[15]D. M. Irber, F. Poggiali, F. Kong, M. Kieschnick, T. Lühmann, D. Kwiatkowski, J. Meijer, J. Du, F. Shi, and F. Reinhard, "Robust all-optical single-shot readout of nitrogen-vacancy centers in diamond," Nat. Commun. **12**, 532 (2021).
[16]A. Darafsheh, "Photonic nanojets and their applications," J. Phys. Photonics **3**, 022001 (2021).
[17]L. Robledo, L. Childress, H. Bernien, B. Hensen, P. F. Alkemade, and R. Hanson, "High-fidelity projective read-out of a solid-state spin quantum register," Nature **477**, 574 (2011).
[18]T. Wriedt and A. Doicu, "Light scattering from a particle on or near a surface," Opt. Commun. **152**, 376 (1998).
[19]X. Ma and E. Li, "Scattering of an unpolarized Bessel beam by spheres," Chin. Opt. Lett. **8**, 1195 (2010).
[20]N. Le Thomas, U. Woggon, W. Langbein, and M. V. Artemyev, "Effect of a dielectric substrate on whispering-gallery-mode sensors," J. Opt. Soc. Am. B **23**, 2361 (2006).